Communication in Mathematical Modeling and Applications
http://ntmsci.com/cmma

# A Model for an Application to Biomedical industry through Viscoinelastic nanofluid flow

*P. Priyadharshini*[1], *M. Vanitha Archana*[2], *E.M. Elsayed*[3,*] *and D. Vivek*[4]

[1,2,4]Department of Mathematics, PSG College of Arts and Science, Coimbatore-641014, India
[3]Department of Mathematics, Faculty of Science,King Abdulaziz University, Jeddah 21589, Saudi Arabia

Received: 1 September 2022, Accepted: 24 November 2022
Published online: 22 May 2023.

**Abstract:** Biomedical procedures such as surgical glue, knee replacement surgery, blood diagnostic and many others can exhibit the significance of viscoinelastic behavior with non-Newtonian characteristics is analyzed. The present article addresses the flow design is to accentuate the thermophysical characteristics of electrically conducting viscoinelastic nanofluid flow produced by a stretched surface. The impacts of Brownian motion and thermophoresis on viscoinelastic nanofluid are accounted in the presence of heat and mass transfer convective states. The modeled partial differential equations are transmuted into nonlinear ordinary differential equations employing similarity transformations to facilitate the computation procedure. The solution of the achieved boundary value problem is procured numerically by utilizing a program written with stiffness-switching methodology. The manners of controlling parameters on the fluid velocity, temperature, and concentration profiles are spotlighted via graphs. Finally, by changing the pertinent parameters, the Machine Learning technique is used to investigate critical properties of fluid flow, such as skin friction coefficient, Nusselt number, and Sherwood number. The effects of driving parameters are illustrated in a graphical and tabular format. The precision of the current methodology is validated by a comparison between the current and previous findings.

**Keywords:** Magnetohydrodynamic, Viscoinelastic Nanofluid, Stretching Sheet, Machine Learning Algorithms.

## 1 Introduction

The heat transfer phenomenon is caused by a temperature distinction between two different bodies. A Prandtl-Eyring nanofluid with heat and mass transfers is particularly essential in metallurgy, solar collectors, combustion systems, chemical engineering, nuclear reactor safety, and other engineering applications. The buoyant forces from both thermal and mass diffusion in heating and cooling caverns, energy phenomena, space technology, and solar power techniques, among other things, govern such transport processes. Inspired by such observations, various researchers are still discussing the heat and mass transfer effects in flow over a stretched surface with radiation effect [17,11,22,21,25,36]. The heat transmission process with convective temperature conditions at the surface is examined in [6,26,27,28,5,14, 24,33,12,16].

Fluids that are commonly encountered in daily life do not act as Newton predicted, i.e., deformation rate does not vary linearly as shear stress accumulations. Blood, toothpaste, paints, ketchup, lubricants, and suspensions are all examples of this sort of fluid. They are called non-Newtonian fluids. The deformation rate is used to estimate the shear characteristics in Newtonian fluids, but this notion fails in non-Newtonian fluids. Non-Newtonian fluids are classified into viscoelastic and viscoinelastic. The current research focuses on the investigation of viscoinelastic fluids. At zero shear stress, most viscoinelastic fluids have similar properties. but on the other hand, properties are extremely unexpected when exposed to stress. Researchers suggested several models for better understanding the physical characteristics of viscoinelastic fluids,

* Corresponding author e-mail: emmelsayed@yahoo.com

including the power-law model, Prandtl fluid model, and Prandtl-Eyring fluid model. The Prandtl-Eyring fluid model is the subject of this investigation. The Prandtl-Eyring nanofluid model has only been used in a few studies for example [4, 2, 8, 10, 19].

Machine learning is a branch of artificial intelligence that emphasizes the construction of computer programmes with data access by allowing the system to enhance and develop automatically by finding patterns in the database without a need for human involvement. In the previous two decades, exabytes of data have been generated, and almost every industry has been digitized. This data is used by machine learning algorithms to build a predictive model and to automate a variety of time-consuming activities. It is divided into three categories: Supervised Machine Learning [23], Unsupervised Machine Learning [15], and Semi-supervised Machine Learning, depending on the data type. The connection between machine learning and fluid mechanics has a fascinating backstory. Applications of wind energy [9, 18, 35, 34, 31, 30], solar energy [37, 32], and renewable energy systems in general [20] demonstrated by using a machine learning approaches. Brenner et al. [7] investigated the role of machine learning in the advancement of fluid mechanics. Rosenblatt's perceptron [29] from the 1950s was designed to emulate the human brain ability to identify a separation hyperplane that splits the training data linearly.

The cesarean delivery method of skin closure glue for wound complications and scar healing (Figure. 2) via viscoinelastic nanofluid flow is investigated. Researchers continue inventing new formulations that display enhanced biocompatibility, stability, elasticity, and degradability. These developments have the potential to enhance clinical outcomes by improving haemorrhage control.

The following is an overview of the paper structure. In Section 2, the modeling statement and mathematical formulation are presented. Section 3 explores the physical quantities of interest. Section 4 explains the solution methodology. The graphical sketches of numerical solutions with physical performance are presented in the final Section. The present investigation is summarised in the conclusion section.

## 2 Flow Analysis

The two-dimensional Prandtl-Eyring nanofluid flow over a stretched sheet is governed by the continuity, Navier–Stokes equations, and Buongiorno design. The velocity of the sheet along the $x$-direction is $U(x) = ax$. A transversely headed magnetic field containing strength $B_0$ is executed to direct the flow direction, as displayed in Figure. 1c. Governing equations for Prandtl-Eyring nanofluid model after concerning the boundary layer approximations can be depicted as

$$\frac{\partial u}{\partial x} + \frac{\partial v}{\partial y} = 0, \tag{1}$$

$$u\frac{\partial u}{\partial x} + v\frac{\partial u}{\partial y} = \frac{A}{\rho c}\frac{\partial^2 u}{\partial y^2} - \frac{A}{2\rho c^3}\left(\frac{\partial u}{\partial y}\right)^2 \frac{\partial^2 u}{\partial y^2} - \frac{\sigma B_0^2}{\rho}u, \tag{2}$$

$$u\frac{\partial T}{\partial x} + v\frac{\partial T}{\partial y} = \alpha_1\left(\frac{\partial^2 T}{\partial y^2}\right) + \tau\left\{D_B\left(\frac{\partial C}{\partial y}\frac{\partial T}{\partial y}\right) + \frac{D_T}{T_\infty}\left(\frac{\partial T}{\partial y}\right)^2\right\}, \tag{3}$$

$$u\frac{\partial C}{\partial x} + v\frac{\partial C}{\partial y} = D_B\left(\frac{\partial^2 C}{\partial y^2}\right) + \frac{D_T}{T_\infty}\left(\frac{\partial^2 T}{\partial y^2}\right), \tag{4}$$

in addition to the boundary constraints

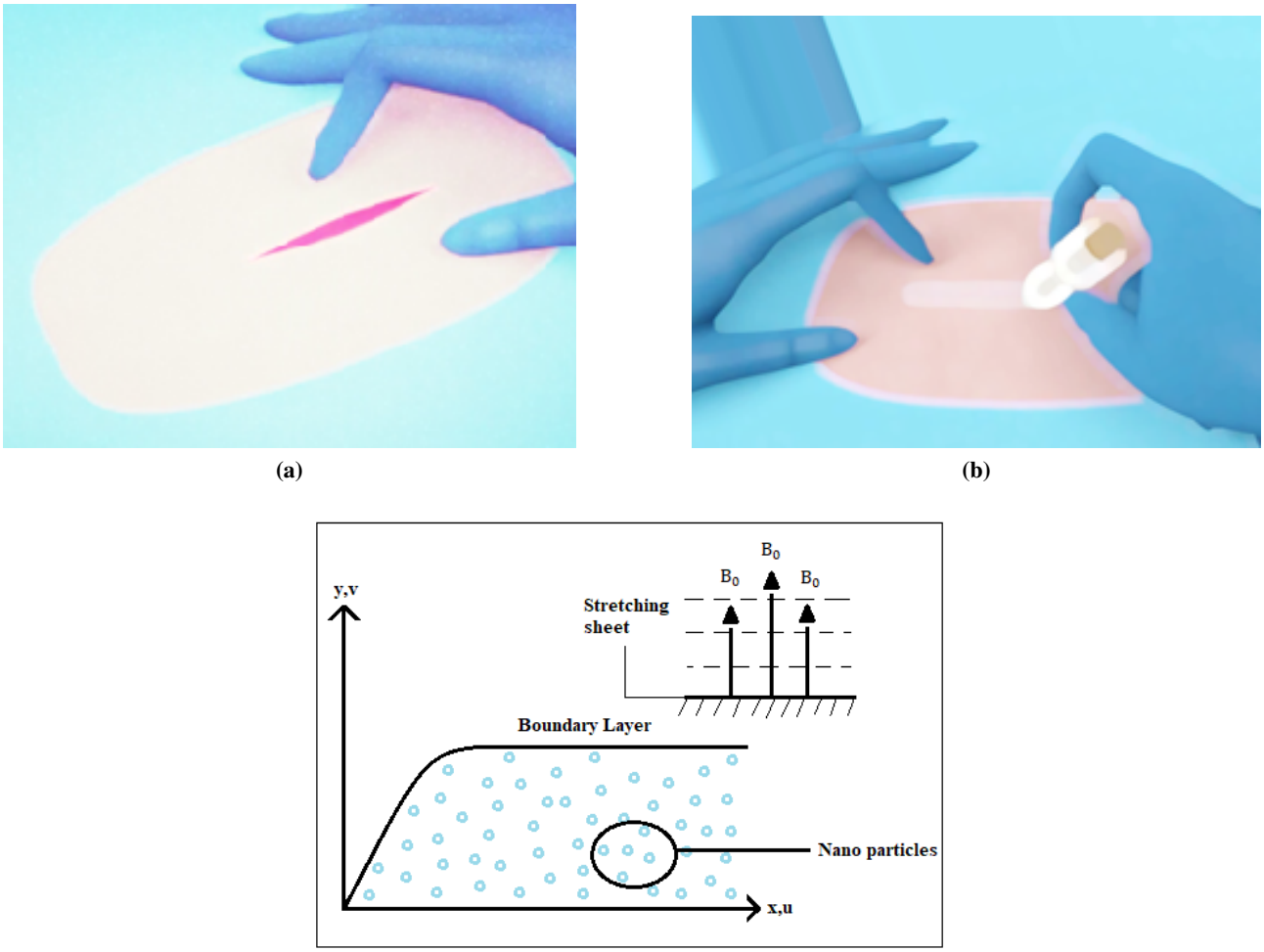


**Fig. 1:** Surgical glue (a) before use (b) applied by connecting the skin edges (c) diagram of flow configuration.

$$\begin{cases} u = U(x),\ v = 0,\ T = T_w \text{ and } C = C_w \text{ at } y = 0; \\ u \to 0,\ T \to T_\infty \text{ and } C \to C_\infty \text{ at } y \to \infty. \end{cases} \tag{5}$$

In the above problem, velocity components along the $x$ and $y$-directions are $u$ and $v$, respectively, $\nu$ is the kinematic viscosity, $\sigma$ is the electrical conductivity, $\rho$ is the density of the fluid. The fluid temperature is $T$, while the ratio between efficient heat range of the nanoparticle material and efficient heat range of the base fluid is $\tau$, $A$ is the material parameter, $c$ is the material parameter, $\alpha_1$ is the thermal diffusivity, $C$ is the nanoparticle concentration particles, $D_B$ is the Brownian diffusion coefficient, $D_T$ is the thermophoresis coefficient. The scaling group of transformations that converted the

governed partial differential equations (1-4) into ordinary differential equations are described below;

$$\begin{cases} \eta = \left(\frac{a}{v}\right)^{\frac{1}{2}} y, \;\; \psi(x,y) = (av)^{\frac{1}{2}} x f(\eta), \\ \theta(\eta) = \frac{T-T_\infty}{T_w - T_\infty}, \;\; \phi(\eta) = \frac{C-C_\infty}{C_w - C_\infty}. \end{cases} \tag{6}$$

Using Equation (6) in (1-4), gives

$$\alpha f'''(\eta) - \alpha\beta f''(\eta)^2 f'''(\eta) - f'(\eta)^2 + f(\eta) f''(\eta) - M f'(\eta) = 0, \tag{7}$$

$$\theta''(\eta) + Pr\left[f(\eta)\theta'(\eta) + Nb\theta'(\eta)\phi'(\eta) + Nt\theta'(\eta)^2\right] = 0, \tag{8}$$

$$\phi''(\eta) + LePr f(\eta)\phi'(\eta) + \frac{Nt}{Nb}\theta''(\eta) = 0, \tag{9}$$

along with the boundary conditions

$$\begin{cases} f(0) = 0, \; f'(0) = 1, \; f'(\infty) = 0; \\ \theta(0) = 1, \; \theta(\infty) \to 0; \\ \phi(0) = 1, \; \phi(\infty) \to 0. \end{cases} \tag{10}$$

Here the Prandtl-Eyring parameters are signified by $\alpha = \frac{A}{\mu c}$ and $\beta = \frac{a^3 x^2}{2c^2 v}$, while the Hartmann number, Brownian motion parameter, thermophoresis parameter, Lewis number, and Prandtl number are $M = \frac{\sigma B^2}{a\rho}$, $Nb = \frac{\tau D_B (C_w - C_\infty)}{v}$, $Nt = \frac{\tau D_T (T_w - T_\infty)}{T_\infty v}$, $Le = \frac{\alpha_1}{D_B}$, and $Pr = \frac{v}{\alpha_1}$, respectively.

## 3 Physical Quantities

The physical quantities of interest, i.e., wall drag coefficient, wall heat, and mass fluxes are defined as

$$C_{fx} = \frac{\tau w}{\frac{1}{2}\rho U^2}, \; Nu_x = \frac{x q_w}{k(T_w - T_\infty)}, \; Sh_x = \frac{x q_m}{D_B (C_w - C_\infty)}. \tag{11}$$

The mathematical expressions of wall shear stress $\tau_w$, wall heat gradient $q_w$ and wall mass gradient $q_m$ is given by,

$$\begin{cases} \tau_w = \frac{A}{c}\left(\frac{\partial u}{\partial y}\right)_{y=0} - \frac{A}{6c^3}\left(\frac{\partial u}{\partial y}\right)^3_{y=0}, \; q_w = -k\left(\frac{\partial T}{\partial Y}\right)_{y=0}, \\ q_m = -D_B\left(\frac{\partial C}{\partial Y}\right)_{y=0}. \end{cases} \tag{12}$$

After comprising the dimensionless variables in equations (11, 12), the skin friction coefficient, Nusselt number, and Sherwood number are acclimated in the subsequent form:

$$\begin{cases} \frac{1}{2} C_{fx} Re_x^{\frac{1}{2}} = \alpha f''(0) - \frac{\alpha\beta}{3}[f''(0)]^3, \; \frac{Nu_x}{Re_x^{\frac{1}{2}}} = -\theta'(0), \\ \frac{Sh_x}{Re_x^{\frac{1}{2}}} = -\phi'(0). \end{cases} \tag{13}$$

| $M$ | Fatehzadeh et al. [13] | Zahra et al. [1] | Akbar et al. [3] | Present results |
|---|---|---|---|---|
| 0 | -1 | -1.004 | 1 | -1.0014 |
| 0.5 | - | -1.1180 | -1.11803 | -1.22491 |
| 1.0 | -1.41412 | -1.4140 | -1.41421 | -1.41424 |
| 5.0 | -2.44948 | -2.4494 | -2.44949 | -2.44949 |
| 10 | -3.31662 | -3.3168 | -3.31663 | -3.31662 |
| 50 | -7.14142 | -4.4143 | - | -7.14143 |
| 100 | -10.0499 | -10.0502 | -10.04988 | -10.0499 |

**Table 1:** Comparision result of skin friction coefficient for various values of Hartmann parameter $M$ when $\alpha$=1, $\beta$=0.

## 4 Solution Methodology

Using a Wolfram Language program, the ordinary differential equations (7-9) are scrutinized numerically with the given boundary constraints (10) for different values of pertinent parameters. Such as Prandtl-Eyring parameters, Hartmann parameter, Brownian motion parameter, thermophoresis parameter, Prandtl number, and Lewis number. Except for the different values of physical parameters shown in distinct figures and tables, the entire computational analysis is the same.

### *4.1 Machine Learning*

The main focus of this study is on supervised learning algorithms, which is a common technique. To learn the input-output mapping function $y_{(pred)} = f$, input variables $x$ and output variables $y_{(pred)}$ are used in pairs $(x)$. The stochastic gradient descent algorithm is one of the most often used forms of the gradient descent approach, as indicated by the above-mentioned fundamentals. The best fit line for the variation of Skin friction coefficient, local Nusselt number and local Sherwood number for a large variety of Hartmann parameter and Prandtl number, are acquired by utilizing Python Language. If $y_{(pred)}, x, b$, and $m$ are the predicted variable, input variable, bias term, and weight of the variable in a simple regression model, then:

$$y_{(pred)} = mx + b$$

When the model is being trained, the mean square error (MSE) is calculated, and it is a useful metric for predicting the fluid flow characteristics, which is almost matches the actual value $(y)$. In each iteration, the error values are minimized. Furthermore, the training process is repeated until the best fit line is discovered.

| **Physical Quantites** | **Parameter Values** | | **Numerical Value** | **Predicted Value** |
|---|---|---|---|---|
| $C_{fx}$ | $\alpha$=1, $\beta = 0$, $Nb = Nt$=0.1, $Pr$=2.0, $Le$=3.0 | M=0 | -1.0014 | -1.06567 |
| | | M=0.5 | -1.22491 | -1.20566 |
| | | M=1 | -1.41424 | -1.34565 |
| | | M=5 | -2.44949 | -2.46553 |
| $Nu_x$ | $\alpha$=1.5, $\beta = 0.1$, $Nb = Nt$=0.1, $M$=0.3, $Le$=3.0 | $Pr$=2 | 0.7694 | 0.75733 |
| | | $Pr$=5 | 1.11067 | 1.00571 |
| | | $Pr$=7 | 1.22577 | 1.17130 |
| | | $Pr$=10 | 1.32562 | 1.41968 |
| $Sh_x$ | $\alpha$=1.5, $\beta = 0.1$, $Nb = Nt$=0.1, $M$=0.3, $Le$=3.0 | $Pr$=2 | 1.47834 | 1.47172 |
| | | $Pr$=5 | 2.73039 | 2.60302 |
| | | $Pr$=7 | 3.4276 | 3.35722 |
| | | $Pr$=10 | 4.37306 | 4.48852 |

**Table 2:** Numerical and predicted value for physical quantities with various parameters.

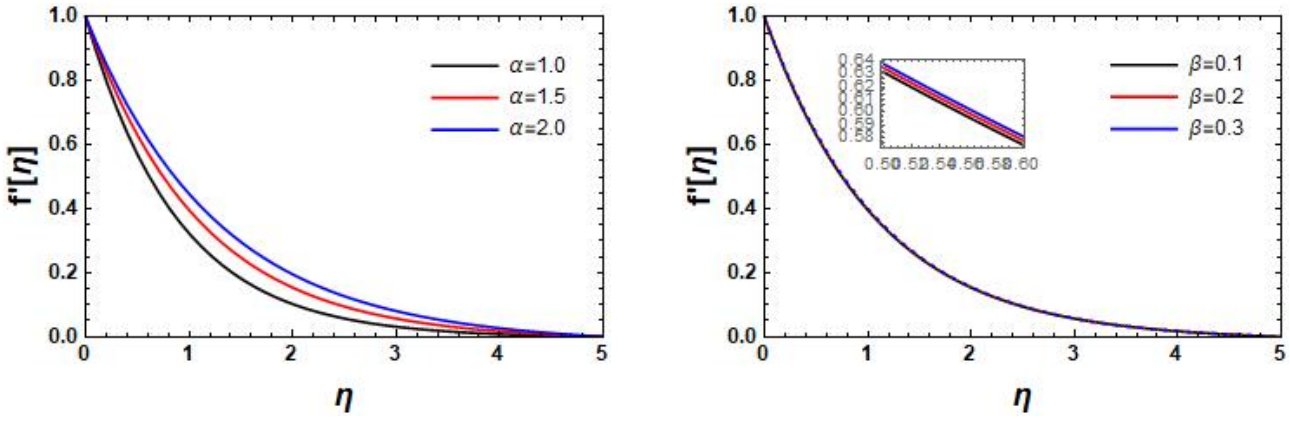


(a) (b)

**Fig. 2:** Influence of (a) fluid parameter $\alpha$ (b) fluid parameter $\beta$ on velocity profile.

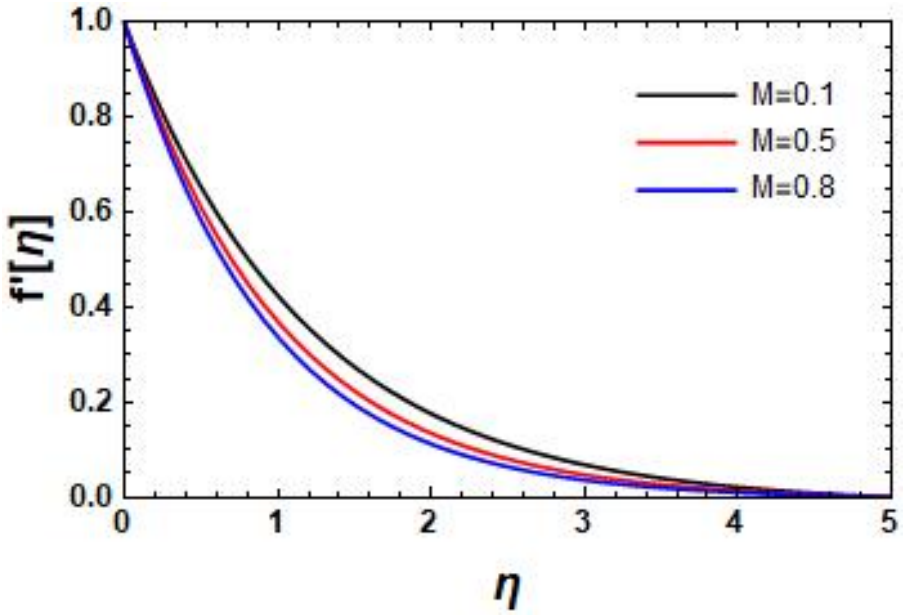


**Fig. 3:** Influence of Hartmann parameter $M$ on velocity profile.

## 5 Graph Findings and Discussion

The main objective of this part is to analyze the outcomes of various pertinent parameters on the velocity field, temperature, and mass concentration fields. $\alpha$=1.5, $\beta$=0.1, $M$=0.3, $Nb$=0.1, $Nt$=0.1, and $Le$=3.0 are the default values, and all graphs adhere to these values unless otherwise mentioned on the graph.

### *5.1 Velocity Profile*

Figure. 2a indicates that the Prandtl-Eyring fluid parameter $\alpha$, accelerates the linear momentum of fluid flow in boundary layer regime, besides for $\alpha > 1$, an enormous boost is detected in fluid velocity. Because, higher values of the pertinent

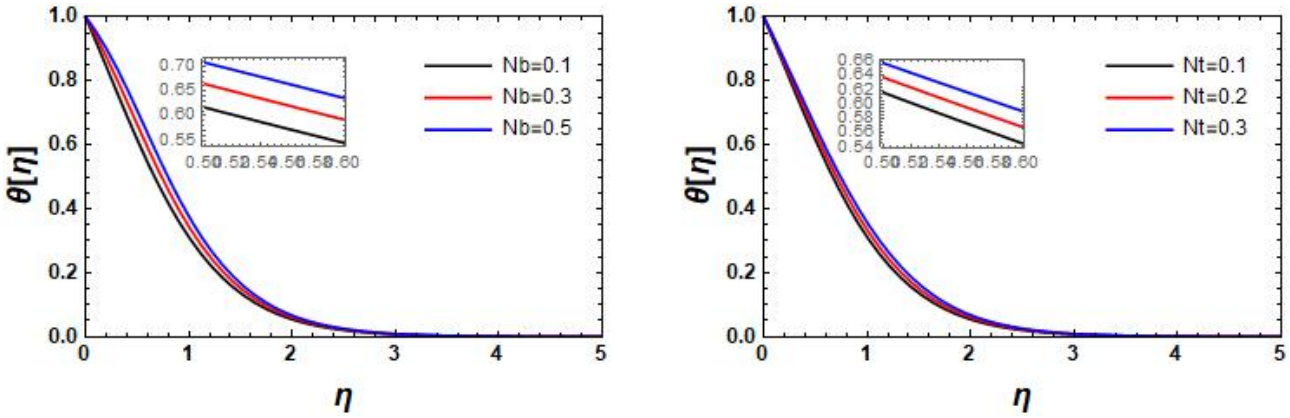


**Fig. 4:** Influence of (a) Brownian motion parameter *Nb* (b) thermophoresis parameter *Nt* on temperature profile.

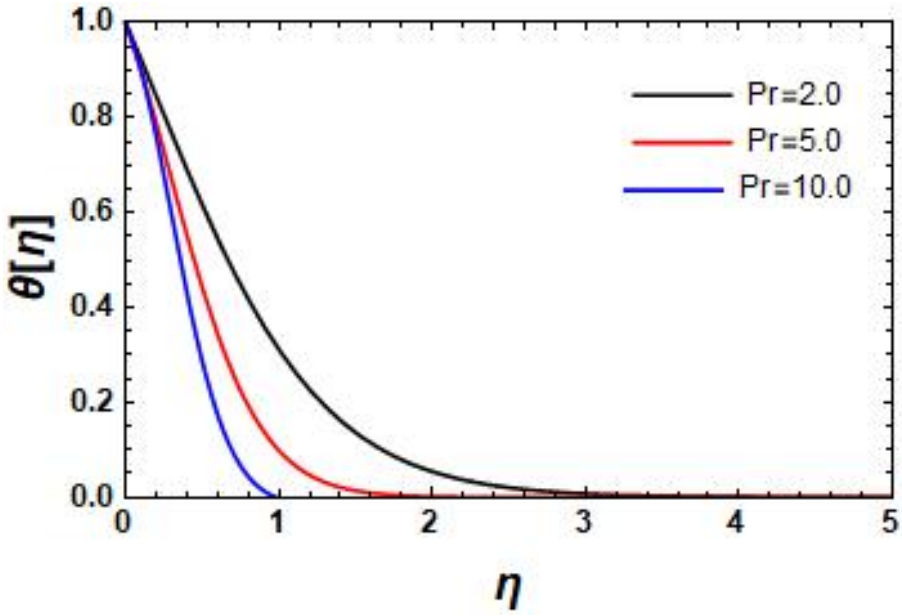


**Fig. 5:** Influence of Prandtl number *Pr* on temperature profile.

parameter $\alpha$ lessen the viscous force. The momentum boundary layer slightly expanded for higher values of a material parameter $\alpha$.

Figure. 2b ensure the impact of fluid parameter $\beta$ on velocity profile. The velocity curves overlap each other, indicating that the velocity profile has altered slightly due to fluid parameter $\beta$ adjustment. Furthermore, this diagram depicted a decrease in linear momentum within boundary layer thickness.

The impact of the Hartmann number $M$ on fluid velocity is adorned in Figure. 3. This graph demonstrated that the velocity curves display decimation versus independent variable $\eta$, further strengthening the transverse magnetic field impact velocity of the flow decreases. This outcome provides strength to the prominent fact that the magnetic field yields Lorentz force, which lessens the velocity profile.

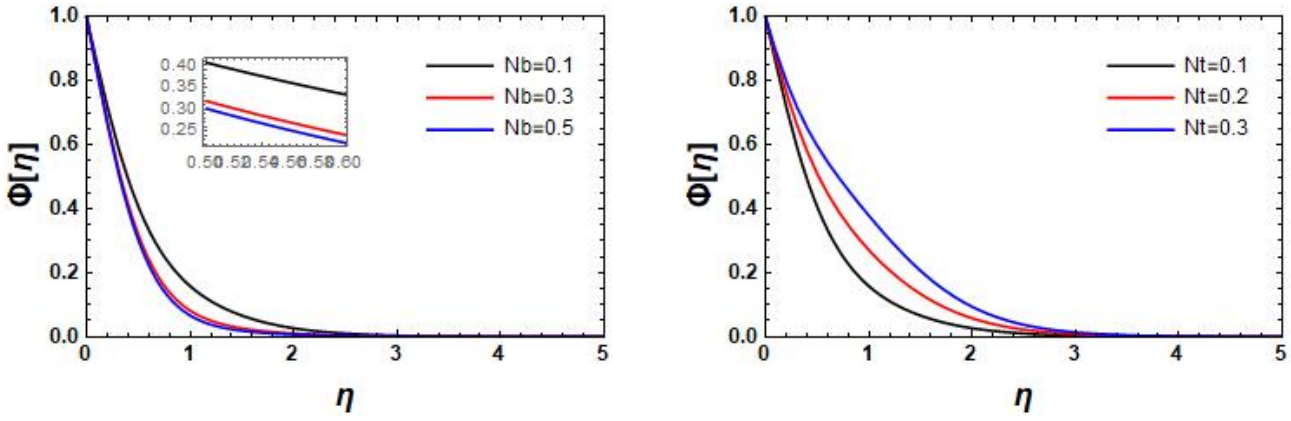


**Fig. 6:** Influence of (a) Brownian motion parameter *Nb* (b) thermophoresis parameter *Nt* on concentration profile.

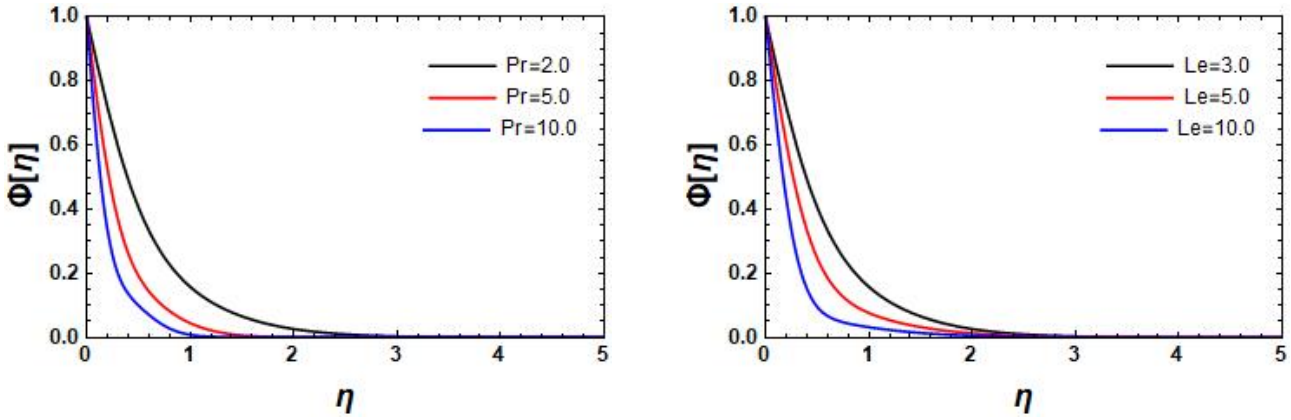


**Fig. 7:** Influence of (a) Prandtl number *Pr* (b) Lewis number *Le* on concentration profile.

A comparison of the obtained results corresponding to the local wall shear rate (i.e., $\alpha$ =1, $\beta$=0) with the existing literature [13,1,3] in Table. 1 is made to validate the accuracy of the proposed numerical scheme and found to be significant agreement.

## *5.2 Temperature and Concentration Profiles*

The fluctuations of Brownian motion parameter *Nb* on temperature profile elucidated in Figure. 4a. The Brownian motion is the movement of nanoparticles in liquids at random. This random movement accelerates the collision of nanoparticles with fluid molecules, and the kinetic energy of the molecules is converted into heat energy, causing the temperature to increase. Also, the thermal boundary layer strip is smaller than the momentum boundary layer strip, as shown in this diagram.

Figure. 4b captures the effect of the thermophoresis parameter *Nt* on the temperature profile. Since the thermophoresis phenomenon causes particles to move faster from a hotter continent to a cooler continent, consequently, heat moves

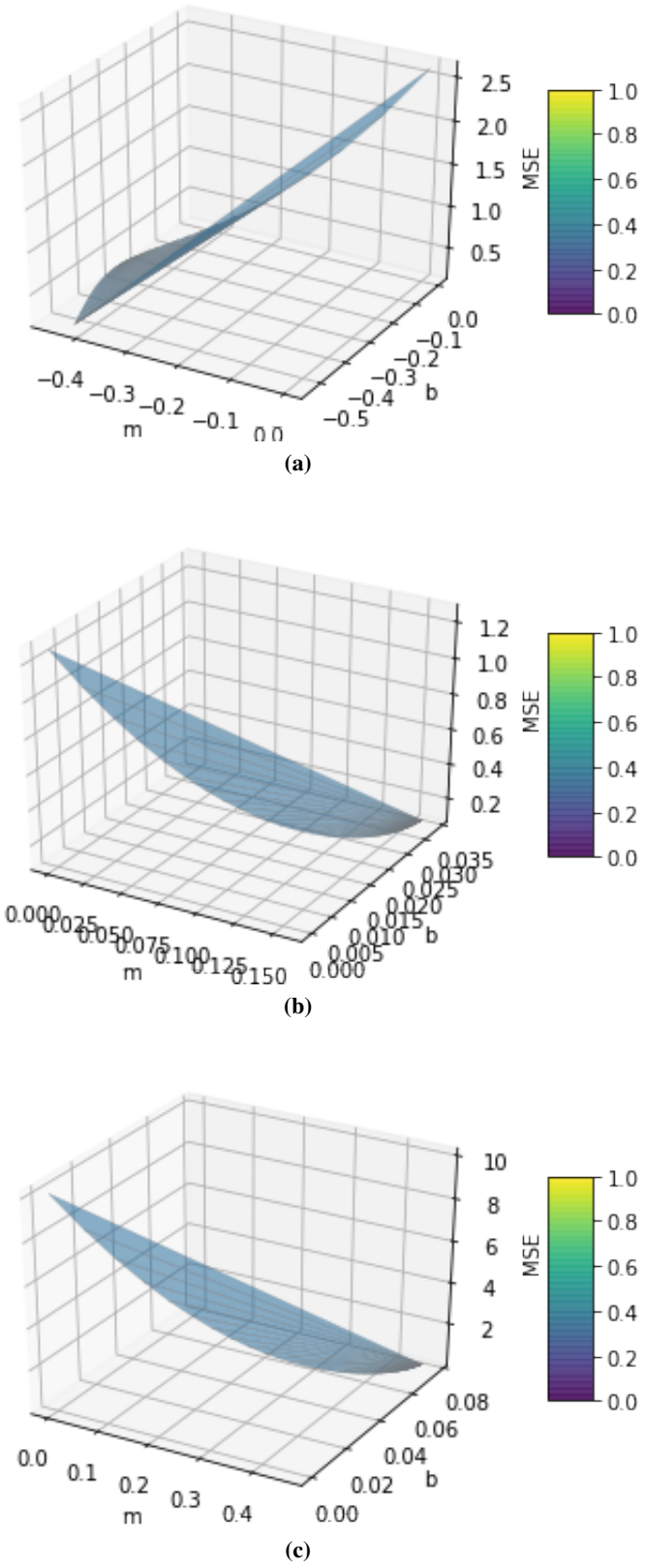


**Fig. 8:** MSE values of (a) Skin friction coefficient against $M$ (b) Nusselt number against $Pr$ (c) Sherwood number against $Pr$.

quickly from hotter surface to fluid. Hence, it raises the temperature. The current figure validated the previously defined theory, and it also shows a gradually rising temperature profile within the thermal boundary layer for given values of thermophoresis parameter.

Figure. 5 displays the impact of Prandtl number $Pr$ on temperature field. The correlation of viscous and thermal conductivity is represented by the Prandtl number. As a consequence, a fluid with a higher Prandtl number has a lower thermal thermal conductivity. The current computed results attest to this fact (Figure. 5). In this figure, it can be seen that temperature decreases significantly in the boundary layer system since Prandtl number increases. Furthermore, a slight decrease in the thermal boundary layer is observed for higher values of Prandtl number.

The effects of Brownian motion parameter $Nb$ on nanoparticle concentration in the boundary layer domain are displayed in Figure. 6a. The graph demonstrates that the Brownian motion lessens both concentration and boundary layer thickness. This is because an increase in Brownian motion accelerates random movement, which evaporates the nanoparticles and thus declines concentration. Figure. 6b demonstrates the effects of thermophoresis parameter $Nt$ on concentration profile. The concentration field rises fast at higher values of the thermophoresis parameter at all points of the flow domain, as seen in this graph.

Figure. 7a sketches the impact of Prandtl number $Pr$ in concentration profile. This graph shows the Prandtl number significantly reduces the nanoparticle concentration. In addition, the boundary layer strip is too thin when the Prandtl number is high. The effects of Lewis number on the concentration profile are elucidated in Figure. 7b. By the definition of Lewis number, higher values of Lewis number decreases the mass diffusivity and thus concentration. This figure forecasts the concentration of nanoparticles, and the thickness of the boundary layer decreases significantly as the Lewis number increases.

Finally, Figure. 8a, 8b, and 8c illustrate the effect of the coefficient of skin friction, Nusselt number, and sherwood number on the broad ranges of Hartmann parameter $M$ and Prandtl number $Pr$ with MSE. Furthermore, Table. 2 clarifies the numerical and estimated model results for numerous testing data sets. The expected outcomes perfectly resemble the numerical value. Thus, the developed model can precisely predict the physical quantities of interest.

## 6 Enumerated Key points

Thermophysical properties of a Prandtl-Eyring nanofluid over a stretched surface are investigated. A program designed in Wolfram Language and machine learning techniques are used to analyze numerical solutions. The following are the specific conclusions reached as a result of application to biomedical industry:

- –The Prandtl-Eyring fluid parameter $\beta$ and the Hartmann number $M$ have an identical influence on fluid velocity. Both parameters lessen velocity, but the Prandtl-Eyring fluid parameter $\alpha$ drives it to increase.
- –Brownian motion and thermophoresis characteristics are favorable for temperature rise, and the Prandtl number reduces the temperature.
- –When Brownian motion diffusion is increased in the boundary layer domain, nanoparticle concentration rises. While the thermophoresis parameter reduces it. Furthermore, the Lewis number and the Prandtl number drastically decrease the concentration.
- –The Machine Learning approach utilized in this work performed well in predicting the nature of physical body through skin friction coefficient, local Nusselt number, and local Sherwood number.

## Data Availability Statement

The data used to support the findings of this study are included within the article.

## Acknowledgments

The authors are grateful to the referees for their educative and constructive comments that refined the paper.

## Conflict of interest

The authors declare that they have no known competing financial interests or personal relationships that could have appeared to influence the work reported in this paper.

## References

[1] Zahra Abdelmalek, Arif Hussain, S Bilal, El-Sayed M Sherif, and Phatiphat Thounthong. Brownian motion and thermophoretic diffusion influence on thermophysical aspects of electrically conducting viscoinelastic nanofluid flow over a stretched surface. *Journal of Materials Research and Technology*, 9(5):11948–11957, 2020.

[2] Noreen Sher Akbar. Mhd eyring–prandtl fluid flow with convective boundary conditions in small intestines. *International Journal of Biomathematics*, 6(05):1350034, 2013.

[3] Noreen Sher Akbar, Abdelhalim Ebaid, and ZH Khan. Numerical analysis of magnetic field effects on eyring-powell fluid flow towards a stretching sheet. *Journal of magnetism and Magnetic Materials*, 382:355–358, 2015.

[4] Noreen Sher Akbar, S Nadeem, and Changhoon Lee. Biomechanical analysis of eyring prandtl fluid model for blood flow in stenosed arteries. *International Journal of Nonlinear Sciences and Numerical Simulation*, 14(6):345–353, 2013.

[5] A Alsaedi, M Awais, and T Hayat. Effects of heat generation/absorption on stagnation point flow of nanofluid over a surface with convective boundary conditions. *Communications in Nonlinear Science and Numerical Simulation*, 17(11):4210–4223, 2012.

[6] Abdul Aziz. A similarity solution for laminar thermal boundary layer over a flat plate with a convective surface boundary condition. *Communications in Nonlinear Science and Numerical Simulation*, 14(4):1064–1068, 2009.

[7] MP Brenner, JD Eldredge, and JB Freund. Perspective on machine learning for advancing fluid mechanics. *Physical Review Fluids*, 4(10):100501, 2019.

[8] Tuncer Cebeci and Peter Bradshaw. *Physical and computational aspects of convective heat transfer*. Springer Science & Business Media, 2012.

[9] A Clifton, L Kilcher, JK Lundquist, and P Fleming. Using machine learning to predict wind turbine power output. *Environmental research letters*, 8(2):024009, 2013.

[10] R. M. Darji and M. G. Timol. • similarity solutions of laminar incompressible boundary layer equations of non-newtonian viscoinelastic fluids. *International Journal of Mathematical Archive*, 2, 2011.

[11] K Das. Effect of chemical reaction and thermal radiation on heat and mass transfer flow of mhd micropolar fluid in a rotating frame of reference. *International journal of heat and mass transfer*, 54(15-16):3505–3513, 2011.

[12] Kalidas Das, Pinaki Ranjan Duari, and Prabir Kumar Kundu. Numerical simulation of nanofluid flow with convective boundary condition. *Journal of the Egyptian Mathematical Society*, 23(2):435–439, 2015.

[13] M Fathizadeh, M Madani, Yasir Khan, Naeem Faraz, Ahmet Yıldırım, and Serap Tutkun. An effective modification of the homotopy perturbation method for mhd viscous flow over a stretching sheet. *Journal of King Saud University-Science*, 25(2):107–113, 2013.

[14] MAA Hamad, Md J Uddin, and AI Md Ismail. Investigation of combined heat and mass transfer by lie group analysis with variable diffusivity taking into account hydrodynamic slip and thermal convective boundary conditions. *International Journal of Heat and Mass Transfer*, 55(4):1355–1362, 2012.

[15] Trevor Hastie, Robert Tibshirani, Jerome H Friedman, and Jerome H Friedman. *The elements of statistical learning: data mining, inference, and prediction*, volume 2. Springer, 2009.

[16] T Hayat, Z Iqbal, M Mustafa, and A Alsaedi. Momentum and heat transfer of an upper-convected maxwell fluid over a moving surface with convective boundary conditions. *Nuclear Engineering and Design*, 252:242–247, 2012.

[17] T Hayat, M Mustafa, and I Pop. Heat and mass transfer for soret and dufour's effect on mixed convection boundary layer flow over a stretching vertical surface in a porous medium filled with a viscoelastic fluid. *Communications in Nonlinear Science and Numerical Simulation*, 15(5):1183–1196, 2010.

[18] Justin Heinermann and Oliver Kramer. Machine learning ensembles for wind power prediction. *Renewable Energy*, 89:671–679, 2016.

[19] Arif Hussain, MY Malik, M Awais, T Salahuddin, and S Bilal. Computational and physical aspects of mhd prandtl-eyring fluid flow analysis over a stretching sheet. *Neural Computing and Applications*, 31(1):425–433, 2019.

[20] Soteris Kalogirou. *Artificial intelligence in energy and renewable energy systems*. Nova Publishers, 2007.

[21] R Kandasamy, T Hayat, and S Obaidat. Group theory transformation for soret and dufour effects on free convective heat and mass transfer with thermophoresis and chemical reaction over a porous stretching surface in the presence of heat source/sink. *Nuclear Engineering and Design*, 241(6):2155–2161, 2011.

[22] F Khani, Abdul Aziz, and S Hamedi-Nezhad. Simultaneous heat and mass transfer in natural convection about an isothermal vertical plate. *Journal of King Saud University-Science*, 24(2):123–129, 2012.

[23] Sotiris B Kotsiantis, Ioannis Zaharakis, P Pintelas, et al. Supervised machine learning: A review of classification techniques. *Emerging artificial intelligence applications in computer engineering*, 160(1):3–24, 2007.

[24] Oluwole D Makinde and A Aziz. Boundary layer flow of a nanofluid past a stretching sheet with a convective boundary condition. *International Journal of Thermal Sciences*, 50(7):1326–1332, 2011.

[25] Dulal Pal and Sewli Chatterjee. Soret and dufour effects on mhd convective heat and mass transfer of a power-law fluid over an inclined plate with variable thermal conductivity in a porous medium. *Applied Mathematics and Computation*, 219(14):7556–7574, 2013.

[26] Prabhugouda Mallangaouda Patil, E Momoniat, and S Roy. Influence of convective boundary condition on double diffusive mixed convection from a permeable vertical surface. *International Journal of Heat and Mass Transfer*, 70:313–321, 2014.

[27] GK Ramesh and BJ Gireesha. Influence of heat source/sink on a maxwell fluid over a stretching surface with convective boundary condition in the presence of nanoparticles. *Ain Shams Engineering Journal*, 5(3):991–998, 2014.

[28] AM Rashad, AJ Chamkha, and M Modather. Mixed convection boundary-layer flow past a horizontal circular cylinder embedded in a porous medium filled with a nanofluid under convective boundary condition. *Computers & Fluids*, 86:380–388, 2013.

[29] Frank Rosenblatt. The perceptron: a probabilistic model for information storage and organization in the brain. *Psychological review*, 65(6):386, 1958.

[30] Mostafa A Rushdi, Ahmad A Rushdi, Tarek N Dief, Amr M Halawa, Shigeo Yoshida, and Roland Schmehl. Power prediction of airborne wind energy systems using multivariate machine learning. *Energies*, 13(9):2367, 2020.

[31] Mostafa A Rushdi, Shigeo Yoshida, Koichi Watanabe, and Yuji Ohya. Machine learning approaches for thermal updraft prediction in wind solar tower systems. *Renewable Energy*, 177:1001–1013, 2021.

[32] Navin Sharma, Pranshu Sharma, David Irwin, and Prashant Shenoy. Predicting solar generation from weather forecasts using machine learning. In *2011 IEEE international conference on smart grid communications (SmartGridComm)*, pages 528–533. IEEE, 2011.

[33] SA Shehzad, A Alsaedi, and T Hayat. Three-dimensional flow of jeffery fluid with convective surface boundary conditions. *International Journal of Heat and Mass Transfer*, 55(15-16):3971–3976, 2012.

[34] Zilong Ti, Xiao Wei Deng, and Hongxing Yang. Wake modeling of wind turbines using machine learning. *Applied Energy*, 257:114025, 2020.

[35] Nils André Treiber, Justin Heinermann, and Oliver Kramer. Wind power prediction with machine learning. In *Computational sustainability*, pages 13–29. Springer, 2016.

[36] M Turkyilmazoglu. Multiple solutions of heat and mass transfer of mhd slip flow for the viscoelastic fluid over a stretching sheet. *International Journal of Thermal Sciences*, 50(11):2264–2276, 2011.

[37] Cyril Voyant, Gilles Notton, Soteris Kalogirou, Marie-Laure Nivet, Christophe Paoli, Fabrice Motte, and Alexis Fouilloy. Machine learning methods for solar radiation forecasting: A review. *Renewable Energy*, 105:569–582, 2017.